Spin-Canting-Induced Band Reconstruction in the Dirac Material Ca_{1-x}Na_{x}MnBi_{2}

R. Yang, M. Corasaniti, C. C. Le, Z. Y. Liao, A. F. Wang, Q. Du, C. Petrovic, X. G. Qiu, J. P. Hu, and L. Degiorgi

Spin-canting-induced band reconstruction in the Dirac material Ca$_{1-x}$Na$_x$MnBi$_2$

R. Yang,[1] M. Corasaniti,[1] C. C. Le,[2] Z. Y. Liao,[3, 4] A. F. Wang [†],[5]
Q. Du,[5, 6] C. Petrovic,[5, 6] X. G. Qiu,[3, 4, 7] J. P. Hu,[3, 8, 9] and L. Degiorgi[1]

[1]*Laboratorium für Festkörperphysik, ETH - Zürich, 8093 Zürich, Switzerland*
[2]*Max Planck Institute for Chemical Physics of Solids, Dresden 01187, Germany*
[3]*Beijing National Laboratory for Condensed Matter Physics,*
Institute of Physics, Chinese Academy of Sciences, Beijing 100190, China
[4]*School of Physical Sciences, University of Chinese Academy of Sciences, Beijing 100049, China*
[5]*Condensed Matter Physics and Materials Science Department,*
Brookhaven National Laboratory, Upton NY 11973, USA
[6]*Department of Materials Science and Chemical Engineering,*
Stony Brook University, Stony Brook, New York 11790, USA
[7]*Songshan Lake Materials Laboratory, Dongguan, Guangdong 523808, China*
[8]*Kavli Institute for Theoretical Sciences and CAS Center for Excellence in Topological Quantum Computation,*
University of Chinese Academy of Sciences, Beijing 100190, China
[9]*South Bay Interdisciplinary Science Center, Dongguan, Guangdong Province, China*

(Dated: March 9, 2020)

The ternary AMnBi$_2$ (A= alkaline as well as rare-earth atom) materials provide an arena for investigating the interplay between low-dimensional magnetism of the antiferromagnetic MnBi layers and the electronic states in the intercalated Bi layers, which harbour relativistic fermions. Here, we report on a comprehensive study of the optical properties and magnetic torque response of Ca$_{1-x}$Na$_x$MnBi$_2$. Our findings give evidence for a spin-canting occurring at $T_s \sim 50-100$ K. With the support of first-principles calculations we establish a direct link between the spin-canting and the reconstruction of the electronic band structure, having immediate implications for the spectral weight reshuffling in the optical response, signalling a partial gapping of the Fermi surface, and the dc transport properties below T_s.

Even though topological materials, based on novel Dirac/Weyl quasiparticles as well as Majorana fermions [1–6], are fairly well understood, there is still an ongoing effort to understand related elusive quantum phenomena and their potential applications, when band topology conspires and coexists with magnetic order, as flagged up by the significant anomalous Hall effect and chiral anomalies in Mn$_3$Sn [7, 8] and GdPtBi [9, 10].

Recently, the ternary materials AMnBi$_2$ (A = alkaline as well as rare-earth atom) [11, 12] have attracted special attention as magnetic topological systems because of the antiferromagnetic (AFM) ground state (Fig. 1(a)) [13] in the presence of anisotropic Dirac cones [14, 15], the latter being of relevance for novel electronic devices. The transition Neel temperature (T_N) ranges between 270 and 290 K, with spins along the easy c-axis [16, 17].

As early recognised in EuMnBi$_2$ [18], it has been conjectured that the interlayer magnetic coupling along the c-axis between the Bi square net and AFM order within the MnBi layers parallel to the ab-plane plays a central role and may be even the origin of the bump-like feature in the dc resistivity $\rho(T)$, observed in CaMnBi$_2$ at $T_s \sim$50 K [11, 12, 19]. By substituting Ca with Na, T_s shifts to higher temperatures and the anomaly of $\rho(T)$ is enhanced (Fig. S1(a) in the Supplemental Material, Ref. 20). The underlying mechanism for this anomaly and whether it reveals an interaction between magnetism and Dirac fermions remains nonetheless to be explored in details. While both Ca^{2+} and Na$^+$ are nonmagnetic, the transition at T_s could be the consequence of a spin

reorientation, for instance due to spin-canting or weak ferromagnetic order [11, 14, 19].

In our first attempt [39] to establish a link between the anomaly in $\rho(T)$ and the electronic properties of the title compound, we uncover optical signatures for a partial gapping of the Fermi surface (FS), for energy scales up to 0.2 eV and with onset at T_s. This may reveal the inclination towards a FS instability in topological materials, accompanied by a sizeable depletion of the density-of-states (DOS) at the Fermi level (E_F). The present work intends to precisely address the microscopic origin of the FS gapping. To this goal, we study Ca$_{1-x}$Na$_x$MnBi$_2$ at three dopings ($x = 0$, 0.03 and 0.05) and as a function of temperature (T) with magnetic torque measurements, as well as with the support of first-principles calculations. We provide evidence for a spin-canting occurring at T_s and leading to a remarkable reconstruction of the electronic band structure, with implications on the reshuffling of spectral weight between the intra- and inter-band optical response across T_s, and possibly anticipating the generation of Weyl states.

In order to set the stage for the present work, we first revisit our previous optical results [39]. We focus our attention on the real part $\sigma_1(\omega)$ of the in-plane optical conductivity for the pristine composition ($x = 0$), shown in Fig. 1(b) from 10 to 4 000 cm^{-1} at 50 ($> T_s$) and 10 ($< T_s$) K. A full review of our original optical findings is provided in Ref. 20, which also details their generality for all Na doping. The narrowing with decreasing T of the low-frequency free-carrier response obviously re-
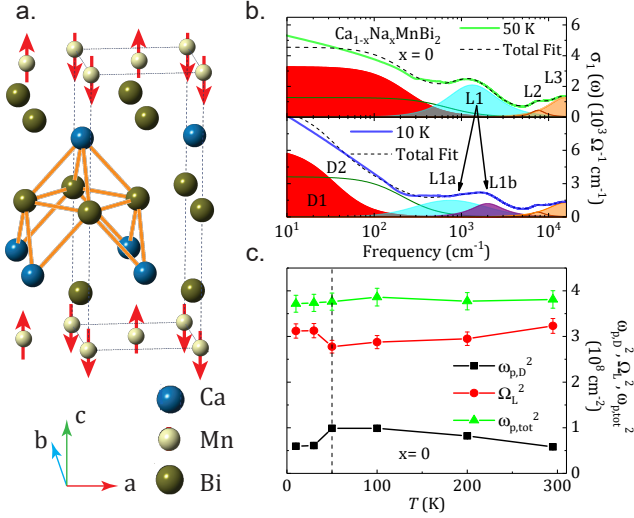
Figure 1. (color online) (a) Crystal structure and C-type AFM order of $Ca_{1-x}Na_xMnBi_2$ (adapted from Ref. 13). (b) Drude-Lorentz fit and its components of $\sigma_1(\omega)$ for $CaMnBi_2$ at $T \gtrless T_s$. Experimental data are partially reproduced from Ref. 39. The fit consists of two Drude terms (D1 and D2), and three additional Lorentz h.o.'s (L1, L2 and L3) [20]. Black arrows denote the split of the MIR peak (h.o. L1 above T_s) into two h.o.'s L1a and L1b below T_s (see text). (c) Spectral weight of the Drude components ($\omega_{p,D}^2 = \omega_{p,D1}^2 + \omega_{p,D2}^2$) and of the MIR Lorentz h.o. ($\Omega_L^2 = \Omega_{L1}^2$ above T_s and $\Omega_L^2 = \Omega_{L1a}^2 + \Omega_{L1b}^2$ below T_s) and of their sum ($\omega_{p,tot}^2 = \omega_{p,D}^2 + \Omega_L^2$), calculated from the fitted strength/plasma frequencies [20].

flects a better coherence with less scattering from thermal fluctuations. Its high-frequency tail then merges into a series of absorptions. The dominant feature, emphasised here, is the mid-infrared (MIR) peak at $\sim 1\,200$ cm^{-1}. We highlight the additional split into two features of this MIR absorption below T_s, which is particularly evident at large Na doping (Figs. S4(a-b) and S5 in Ref. 20) and bears testimony to a remarkable band reconstruction in coincidence with the spin reorientation at T_s.

With the goal to quantitatively describe the electrodynamic response, we expand our previous discussion of the optical data with their fit within the common Drude-Lorentz phenomenological approach [40]. The resulting fits of $\sigma_1(\omega)$ with their constituent components are displayed in Fig. 1(b). We refer to Ref. 20 for details of the fit procedure and parameters. Complementary to our previous analysis of the integrated spectral weight (SW) [39], we can address here the phenomenological one, defined as squared plasma frequency ($\omega_{p,Di}^2$) or oscillator strength (Ω_j^2). This allows us focusing the attention on its reshuffling within selected spectral ranges (i.e., related to each fit component). Figure 1(c) shows the T dependence of the Drude ($\omega_{p,D}^2$) and MIR (Ω_L^2) SW as well as of the total one ($\omega_{p,tot}^2 = \omega_{p,D}^2 + \Omega_L^2$). Since the Lorentz h.o.'s above $4\,000$ cm^{-1} do not show any noteworthy T dependence (Fig. S7 in Ref. 20), the conservation of
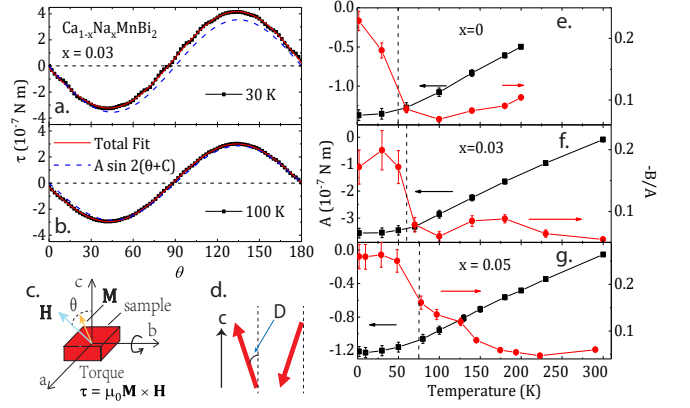

Figure 2. (color online) (a-b) Magnetic torque ($\tau = \mu_0\mathbf{M}\times\mathbf{H}$) as a function of the polar angle (θ) of $x = 0.03$ above and below $T_s \sim 60$ K, respectively. Red curve is the total fit after Eq. 1. We refer to Fig. S8 in Ref. 20 for the comprehensive display of the original data at all Na doping. (c-d) Schematic representations of the experimental configuration for the magnetic torque measurements and the proposed spin-canting. The phase shift D is the canting angle. (e-g) T dependence of the coefficient A (black) and $-B/A$ (red) of Eq. 1 for $x = 0$, 0.03 and 0.05. The vertical dashed lines mark T_s.

SW only requires that $\omega_{p,tot}^2$ remains constant. This is indeed the case in Fig. 1(c), and it phenomenologically emphasises that the reshuffling of SW upon lowering T must essentially occur in the energy interval of about 0.2 eV from E_F between the Drude and MIR contributions in $\sigma_1(\omega)$, suggesting a sizeable T dependence of the electronic band structure also at energy scales relevant for transport [39]. Above T_s, SW of the Drude components increases, while there is a slight suppression of SW in the MIR absorption upon cooling. Since the scattering rates of the Drude components (Fig. S6 in Ref. 20) do not show any remarkable T dependence above T_s, the decreasing resistivity (Fig. S1(a) in Ref. 20) is mainly due to the increasing Drude weight. The reinforcement of the Drude weight at the cost of the MIR inter-band transitions may be the consequence of a reduced Pauli blocking effect upon lowering the chemical potential with decreasing T within the lower Dirac cone [41]. When $T < T_s$, SW of the Drude contribution is partially suppressed, while SW of the MIR harmonic oscillator increases, in broad agreement with our conclusions drawn from the integrated SW [39]. The depletion of the intra-band SW signifies at least a depletion of DOS at E_F below T_s [39], which is also in line with the suppressed thermal conductivity and Hall carrier density observed earlier [19, 20]. In principle, such a reduction of DOS at E_F should result in an increase of $\rho(T)$. However, the scattering rate ($1/\tau$) of the residual Drude components appreciably decreases at low T (Fig. S6 in Ref. 20), so that the competition between $1/\tau$ and DOS leads to a bump-like feature in $\rho(T)$, as observed in Fig. S1(a) in Ref. 20.

In Ref. 39, we advance the scenario that the experimental signatures in $\sigma_1(\omega)$ and $\rho(T)$ of the transition

at T_s are reminiscent of the consequences due to the FS instability, induced by a charge/spin density-wave transition [42]. However, the absence of a jump in the specific heat (Ref. 11 and Fig. S1(b) in Ref. 20), the smooth behaviour of the lattice parameter detected by neutron scattering [16] and the absence of any obvious band-folding in angle-resolved photoemission spectroscopy (ARPES) data [15] tend to a scenario for which the reduction of DOS at E_F (i.e., reduction of the Drude SW below T_s, Fig. 1(c)) is due to a reconstruction of the electronic band structure driven by the spin reorientation itself [43], rather than a density-wave order.

Instrumental in solving this dichotomy is then the magnetic torque ($\tau = \mu_0 \mathbf{M} \times \mathbf{H}$, Ref. 20) experiment. Because of the resolution limit of our commercial instrument at low magnetic fields, we measure the angle-dependence of $\tau(\theta)$ at a relatively high field [20]. We show it below (30 K) and above (100 K) T_s in Figs. 2(a-b), respectively, for $x = 0.03$ as a function of the angle θ between the c-axis and applied field of 3 T (Fig. 2(c)). All curves show roughly a $-sin\,2\theta$ behaviour. However, at $T < T_s$ the discrepancy from the $-sin\,2\theta$ functional is more prominent (Figs. 2(a) and S8 in Ref. 20).

In order to precisely analyse the $\tau(\theta)$ data, we make use of the phenomenological two components fit given by:

$$\tau(\theta) = A sin\,2(\theta + C) + B sin\,(\theta + D),\qquad(1)$$

where the first term refers to the AFM response and the second one stands for the FM contribution, while C and D are the corresponding phase shifts [20, 44–47]. The coefficient A is equal to $\frac{1}{2}\mu_0(\chi_\parallel - \chi_\perp)H^2$ [48]. Since the magnetic moments in $Ca_{1-x}Na_xMnBi_2$ are preferentially aligned along the easy c-axis (Fig. 1(a)) of the AFM state [16], one can set $\chi_\parallel = \chi_c$ and $\chi_\perp = \chi_a$; χ_c and χ_a are the magnetic susceptibility along the c- and a-axis, respectively. The deviation below T_s from the purely AFM response (dashed line in Figs. 2(a-b)) may be accounted for by the second term in Eq. 1, for which $B = \mu_0 M_s H$, where M_s is the saturated magnetisation of the FM response [20, 46]. In Fig. S8 of Ref. 20, the $\tau(\theta)$ data are decomposed after the AFM and FM components. Figures 2(e-g) show the T dependence of the resulting A and $-B/A$ coefficients for all investigated compositions. We choose to show $-B/A$ in order to enhance the (weak) FM contribution over the dominating AFM one. Upon cooling, A is negative and its absolute value progressively increases. The T dependence of A is overall consistent with the magnetic susceptibility of $CaMnBi_2$, for which the in-plane one (χ_a) is almost unchanged, and the out-plane one along the easy axis (χ_c) decreases continuously with lowering T, being both largely shaped by the AFM state [11]. On the contrary, B, being positive and much smaller than $|A|$, moderately increases from 300 K to T_s, which is associated with a weak FM signature, possibly caused by vacancies [20, 43]. Around T_s its enhancement occurs more rapidly, which signifies a net, additional FM response causing the weak bump-like anomaly in χ_c be-

low T_s [11]. The phase shifts C and D are estimated by fit to be 0 and -10.5±2°, respectively [20]. If the FM response is exclusively along the c-axis, the phase shift D should be zero. Therefore, the finite D value signals the presence of a tilting of about 10° of the magnetic moments from the c-axis, as shown in Fig. 2(d), which is particularly relevant below T_s (Fig. S8(d) in Ref. [20]) and gives rise to a canted AFM order. The presence of in-place projected magnetic moments below T_s is also supported by our data collected at fixed angles upon sweeping the magnetic field (Fig. S9 in Ref. 20). It is fair noting that, besides the already mentioned tiny discrepancies from stoichiometry, the spin-flop [49] could also lead to a net FM response. Nonetheless, its absence in the title compound [12], the phase shift $D \neq 0$ itself and the encountered FM behaviour in both the in-plane and out-of-plane susceptibility (Fig. S2 in Ref. 20) further favour the spin-canting scenario, a signature of growing importance in topological magnetic materials [43, 50].

We introduce here the calculation of the electronic band structure of $CaMnBi_2$ based on the density functional theory (DFT), which is of paramount importance towards a comprehensive account of the experimental findings, deployed so far. Figure 3(a) displays the band structure in the C-type AFM state (Fig. 1(a)) without canting, while Fig. 3(b) shows it with 10° canting angle. Upon switching-on the spin-canting, the exchange effect caused by the net FM response leads to a split of almost all bands into spin-up and spin-down dominated branches (Fig. 3(b)). However, near E_F only the hole-like bands from the intercalated Bi p_z orbital (which predominantly hybridises with the Mn $d_{x^2-y^2}$ orbital through the intralayer Bi p_z orbital, Fig. S10 in Ref. 20) are remarkably split, while the linear bands from the intercalated Bi $p_{x/y}$ orbitals are almost unchanged [20]. This means that the $p_{x/y}$ orbitals are marginal to the magnetism in MnBi layers and less sensitive to the net FM order. The consequences of canting are also imaged by the changes of DOS at E_F, shown in Figs. 3(c-e). We observe an overall depletion of DOS at E_F, which mainly affects the p_z orbital contribution (Fig. 3(d)), while negligible variations are encountered at E_F for $p_{x/y}$ orbitals (Fig. 3(e)).

Supported by our first-principles calculations, we propose to interpret the MIR absorption in $\sigma_1(\omega)$ above T_s (Figs. 1(b) and S4(a-b) in Ref. 20) in terms of the inter-band transition between the Mn $d_{x^2-y^2}$-dominated band and the intercalated Bi p_z-dominated hole-pocket around the Γ point of Brillouin zone (BZ), as indicated by the blue arrows in Fig. 3(a) and its inset. Indeed, the calculated (inter-band) optical conductivity $\sigma_1^{inter}(\omega)$ shows an excitation at a similar energy scale (Fig. 3(f)). This absorption reflects the $p - d$ hybridization between Mn and intercalated Bi orbitals, which are involved in the interlayer magnetic coupling. On the other hand, the spin-canting-induced split of the intercalated Bi p_z orbital around the Γ point of BZ (insets of Fig. 3(b)) leads to a shift above E_F of one branch and thus induces a hole pocket (i.e., empty states). The resulting enhanced
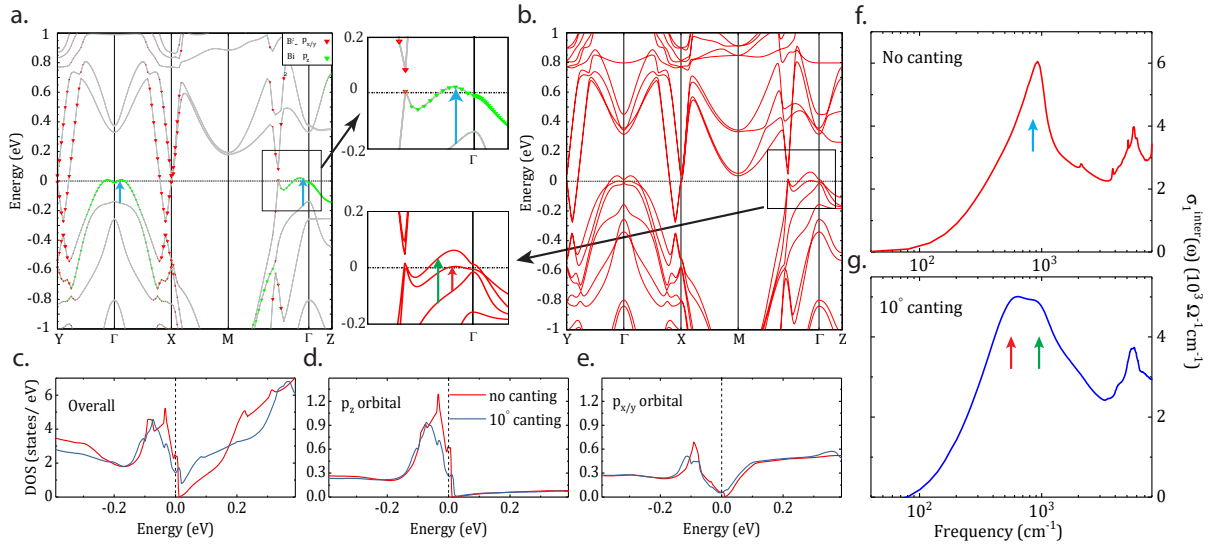
Figure 3. (color online) (a-b) Electronic band structure without (a) and with (b) spin-canting. In (a), the contribution from different Bi p orbitals in the square net are denoted by different colours [20]. Insets: blow-up of the electronic band structure inside the black boxes of the main panels (a) and (b). (c-e) Total density of states (DOS) (c) as well as partial one for p_z (d) and $p_{x/y}$ (e) orbitals. (f-g) Calculated inter-band contribution ($\sigma_1^{inter}(\omega)$) of the optical conductivity [20] from the band structure without (f) and with (g) spin-canting. The arrows in panels (a-b and f-g) (blue without, and red and green after canting) highlight the inter-band transitions responsible for the MIR absorption and its split in $\sigma_1(\omega)$ (Figs. 1(b) and S4(a-b) in Ref. 20).

hole character also generates the possibility for additional inter-band transitions (Fig. 3(b) and its inset). Concomitantly, the MIR feature in $\sigma_1^{inter}(\omega)$ splits into two peaks (indicated by the red and green arrows in Figs. 3(b) and (g)), in excellent agreement with the experimental findings (Figs. 1(b) and S4 in Ref. 20). Moreover, the related reduction of DOS at E_F with spin-canting (Figs. 3(c-e)) foresees the depletion of the Drude-like SW in $\sigma_1(\omega)$ (Fig. 1(c) and Refs. 20 and 39).

So far, we focused the attention on the impact of the experimentally determined spin-canting on the electronic band structure. The outcome of our first-principles calculations similarly catches a glimpse of the driving mechanism leading to the spin-canting itself. We propose that it resides in the interlayer magnetic coupling between the Mn d orbitals, mediated by the p orbitals of the intercalated Bi square nets (Fig. 1(a)). Such a scenario encounters the basic features of the super-exchange magnetic coupling (details in Ref. 20) and may reveal the microscopic origin of the anomaly in $\rho(T)$ and its Na doping dependence. Indeed with Na doping, the reduced interlayer distance enhances the overlap between the Bi p and Mn d orbitals and thus the $p-d$ hopping integral, while more unoccupied states as a consequence of the hole-doping in the Bi p_z orbital should equally reduce the energy difference between the relevant occupied p/d orbitals. All this leads to an enhancement of the interlayer magnetic coupling, which favours a higher transition temperature T_s in accord with $\rho(T)$ of Ca$_{1-x}$Na$_x$MnBi$_2$ (Fig. S1(a) in Ref. 20). Furthermore, we speculate that with a larger hole pocket, as for Na-doped CaMnBi$_2$ because of the

robust downward energy shift of the chemical potential, even more DOS at E_F will be consumed by spin-canting (also irrespective of correlation effects, Fig. S11 in Ref. 20). Thus, a more obvious anomaly may be foreseen in $\rho(T)$, in trend with the experimental observations (Fig. S1(a) in Ref. 20) despite the impact of the decreasing scattering rate at $T < T_s$ (Fig. S6 in Ref. 20).

Finally, we shall compare the title compound with the structurally similar YbMnBi$_2$. Even though they both share the same fingerprints in their electronic band structure, one can notice that in YbMnBi$_2$ all bands around the Γ point are below E_F [50, 51], while those in CaMnBi$_2$ cross E_F. The hopping between the $p-d$ orbitals, introduced above for mediating the magnetic interlayer coupling, is then blocked in YbMnBi$_2$, making the electronic environment for spin-canting less favourable. Moreover, neutron scattering investigations [16, 52] determine a smaller single-ion anisotropy in CaMnBi$_2$ than in YbMnBi$_2$. The smaller the latter parameter is, the weaker the spins will be constrained along the easy c-axis, so that the spin-canting takes place more easily in CaMnBi$_2$.

ARPES investigations on YbMnBi$_2$ [50], though, give evidence for the realisation of a type-II Weyl semimetal and it was claimed that the necessary breaking of the time-reversal-symmetry (TRS) is driven by spin-canting, as well. This is however debated and experimentally controversial. Recent neutron scattering measurements on YbMnBi$_2$ [52] do not detect any fingerprints of spin-canting in the bulk but cannot exclude that it might happen at the sample surface only (where ARPES is sensi-

tive), for instance as a consequence of Yb vacancies. This possibility could reconcile such a variety of yet contrasting data [51].

Obviously, if spin-canting is the principle driving mechanism for the reconstruction of the electronic band structure below T_s, as revealed by our experiments, we might expect the realisation of Weyl states in Na-doped $CaMnBi_2$ as a consequence of the broken TRS. This is of wider interest, because of the peculiar Dirac band crossing along a continuous line in momentum space in $CaMnBi_2$ [53]. There is thus a pressing need for high-resolution ARPES experiments at $T < T_s$ in $Ca_{1-x}Na_xMnBi_2$, paired with neutron scattering investigations on their single crystals.

† Present address: School of Physics, Chongqing University, Chongqing 400044, China

[1] M. Z. Hasan and C. L. Kane, Rev. Mod. Phys. **82**, 3045 (2010).

[2] K. S. Novoselov, A. K. Geim, S. V. Morozov, D. Jiang, M. I. Katsnelson, I. V. Grigorieva, S. V. Dubonos, and A. A. Firsov, Nature (London) **438**, 197 (2005).

[3] C.-Z. Chang, J. Zhang, X. Feng, J. Shen, Z. Zhang, M. Guo, K. Li, Y. Ou, P. Wei, L.-L. Wang, Z.-Q. Ji, Y. Feng, S. Ji, X. Chen, J. Jia, X. Dai, Z. Fang, S.-C. Zhang, K. He, Y. Wang, L. Lu, X.-C. Ma, and Q.-K. Xue, Science **340**, 167 (2013).

[4] J. Li, Y. Li, S. Du, Z. Wang, B.-L. Gu, S.-C. Zhang, K. He, W. Duan, and Y. Xu, Sci. Adv. **5**, eaaw5685 (2019).

[5] X.-L. Qi and S.-C. Zhang, Rev. Mod. Phys. **83**, 1057 (2011).

[6] Q. Wang, Y. Xu, R. Lou, Z. Liu, M. Li, Y. Huang, D. Shen, H. Weng, S. Wang, and H. Lei, Nat. Commun. **9**, 3681 (2018).

[7] A. K. Nayak, J. E. Fischer, Y. Sun, B. Yan, J. Karel, A. C. Komarek, C. Shekhar, N. Kumar, W. Schnelle, J. Kübler, C. Felser, and S. S. P. Parkin, Sci. Adv. **2**, e1501870 (2016).

[8] S. Nakatsuji, N. Kiyohara, and T. Higo, Nature (London) **527**, 212 (2015).

[9] T. Suzuki, R. Chisnell, A. Devarakonda, Y.-T. Liu, W. Feng, D. Xiao, J. W. Lynn, and J. G. Checkelsky, Nat. Phys. **12**, 1119 (2016).

[10] M. Hirschberger, S. Kushwaha, Z. Wang, Q. Gibson, S. Liang, C. A. Belvin, B. A. Bernevig, R. J. Cava, and N. P. Ong, Nat. Mater. **15**, 1161 (2016).

[11] J. B. He, D. M. Wang, and G. F. Chen, Appl. Phys. Lett. **100**, 112405 (2012).

[12] A. Wang, D. Graf, L. Wu, K. Wang, E. Bozin, Y. Zhu, and C. Petrovic, Phys. Rev. B **94**, 125118 (2016).

[13] A. Zhang, C. Liu, C. Yi, G. Zhao, T. L. Xia, J. Ji, Y. Shi, R. Yu, X. Wang, C. Chen, and Q. Zhang, Nat. Commun. **7**, 13833 (2016).

[14] J. Park, G. Lee, F. Wolff-Fabris, Y. Y. Koh, M. J. Eom, Y. K. Kim, M. A. Farhan, Y. J. Jo, C. Kim, J. H. Shim, and J. S. Kim, Phys. Rev. Lett. **107**, 126402 (2011).

[15] Y. Feng, Z. Wang, C. Chen, Y. Shi, Z. Xie, H. Yi, A. Liang, S. He, J. He, Y. Peng, X. Liu, Y. Liu, L. Zhao, G. Liu, X. Dong, J. Zhang, C. Chen, Z. Xu, X. Dai, Z. Fang, and X. J. Zhou, Sci. Rep. **4**, 5385 (2014).

[16] Y. F. Guo, A. J. Princep, X. Zhang, P. Manuel, D. Khalyavin, I. I. Mazin, Y. G. Shi, and A. T. Boothroyd, Phys. Rev. B **90**, 075120 (2014).

[17] M. C. Rahn, A. J. Princep, A. Piovano, J. Kulda, Y. F. Guo, Y. G. Shi, and A. T. Boothroyd, Phys. Rev. B **95**, 134405 (2017).

[18] A. F. May, M. A. McGuire, and B. C. Sales, Phys. Rev. B **90**, 075109 (2014).

[19] K. Wang, L. Wang, and C. Petrovic, Appl. Phys. Lett. **100**, 112111 (2012).

[20] See Supplemental Material at [URL will be inserted by publisher] for further details of the samples characterisation and experimental techniques as well as for complementary data and analysis. It also includes additional Refs. 21–38.

[21] K. Wang, D. Graf, L. Wang, H. Lei, S. W. Tozer, and C. Petrovic, Physical Review B **85**, 041101 (2012).

[22] F. Pfuner, P. Lerch, J.-H. Chu, H.-H. Kuo, I. R. Fisher, and L. Degiorgi, Phys. Rev. B **81**, 195110 (2010).

[23] C. F. Miclea, H. D. Hochheimer, B. Martin, C. Miclea, and T. Ohtani, New J. Phys. **15**, 083008 (2013).

[24] F. Rullier-Albenque, D. Colson, A. Forget, and H. Alloul, Phys. Rev. Lett. **103**, 057001 (2009).

[25] N. P. Ong and P. Monceau, Phys. Rev. B **16**, 3443 (1977).

[26] R. S. Kwok, G. Grüner, and S. E. Brown, Phys. Rev. Lett. **65**, 365 (1990).

[27] D. Starešinić, A. Kiš, K. Biljaković, B. Emerling, J. W. Brill, J. Souletie, H. Berger, and F. Lévy, Eur. Phys. J. B **29**, 71 (2002).

[28] W. Zhang, K. Nadeem, H. Xiao, R. Yang, B. Xu,

H. Yang, and X. G. Qiu, Phys. Rev. B **92**, 144416 (2015).

[29] J. Kanamori, *Magnetism*, edited by H. Suhl and G. T. Rado, Vol. 1 (Academic Press, New York, 1973) Chap. 4.

[30] G. Kresse and J. Hafner, Phys. Rev. B **47**, 558 (1993).

[31] G. Kresse and J. Furthmüller, Comp. Mater. Sci. **6**, 15 (1996).

[32] G. Kresse and J. Furthmüller, Phys. Rev. B **54**, 11169 (1996).

[33] H. J. Monkhorst and J. D. Pack, Phys. Rev. B **13**, 5188 (1976).

[34] P. Blaha, K. Schwarz, P. Sorantin, and S. Trickey, Computer Physics Communications **59**, 399 (1990).

[35] F. J. Ohkawa and N. Matsumoto, J. Phys. Soc. Jap. **63**, 602 (1994).

[36] F. Ma, W. Ji, J. Hu, Z.-Y. Lu, and T. Xiang, Phys. Rev. Lett. **102**, 177003 (2009).

[37] C.-Y. Moon and H. J. Choi, Phys. Rev. Lett. **104**, 057003 (2010).

[38] Z. Wang, P. Zhang, G. Xu, L. K. Zeng, H. Miao, X. Xu, T. Qian, H. Weng, P. Richard, A. V. Fedorov, H. Ding, X. Dai, and Z. Fang, Phys. Rev. B **92**, 115119 (2015).

[39] M. Corasaniti, R. Yang, A. Pal, M. Chinotti, L. Degiorgi, A. Wang, and C. Petrovic, Phys. Rev. B **100**, 041107 (R) (2019).

[40] M. Dressel and G. Grüner, *Electrodynamics of Solids* (Cambridge University Press, Cambridge, 2002).

[41] The spin-orbit coupling gaps the Dirac cones and moves the Fermi level into the lower one [15]. Upon lowering T, the intra-band response is thus more favourable than the excitation across the gapped Dirac cones.

[42] G. Grüner, *Density Waves in Solids*, Advanced book program: Addison-Wesley (Perseus Books Group, 2000).

[43] J. Y. Liu, J. Hu, Q. Zhang, D. Graf, H. B. Cao, S. M. A. Radmanesh, D. J. Adams, Y. L. Zhu, G. F. Cheng, X. Liu, W. A. Phelan, J. Wei, M. Jaime, F. Balakirev, D. A. Tennant, J. F. DiTusa, I. Chiorescu, L. Spinu, and Z. Q. Mao, Nat. Mater. **16**, 905 (2017).

[44] S. Weyeneth, P. J. W. Moll, R. Puzniak, K. Ninios, F. F. Balakirev, R. D. McDonald, H. B. Chan, N. D. Zhigadlo, S. Katrych, Z. Bukowski, J. Karpinski, H. Keller, B. Batlogg, and L. Balicas, Phys. Rev. B **83**, 134503 (2011).

[45] M. D. Watson, A. McCollam, S. F. Blake, D. Vignolles, L. Drigo, I. I. Mazin, D. Guterding, H. O. Jeschke, R. Valentí, N. Ni, R. Cava, and A. I. Coldea, Phys. Rev. B **89**, 205136 (2014).

[46] L. Chen, F. Yu, Z. Xiang, T. Asaba, C. Tinsman, B. Lawson, P. M. Sass, W. Wu, B. L. Kang, X. Chen, and L. Li, Phys. Rev. Applied **9**, 024005 (2018).

[47] H. Xiao, T. Hu, C. C. Almasan, T. A. Sayles, and M. B. Maple, Phys. Rev. B **73**, 184511 (2006).

[48] K. Yosida, Progress of Theoretical Physics **6**, 691 (1951).

[49] H. Masuda, H. Sakai, M. Tokunaga, M. Ochi, H. Takahashi, K. Akiba, A. Miyake, K. Kuroki, Y. Tokura, and S. Ishiwata, Phys. Rev. B **98**, 161108 (2018).

[50] S. Borisenko, D. Evtushinsky, Q. Gibson, A. Yaresko, K. Koepernik, T. Kim, M. Ali, J. van den Brink, M. Hoesch, A. Fedorov, E. Haubold, Y. Kushnirenko, I. Soldatov, R. Schäfer, and R. J. Cava, Nat. Commun. **10**, 3424 (2019).

[51] D. Chaudhuri, B. Cheng, A. Yaresko, Q. D. Gibson, R. J. Cava, and N. P. Armitage, Phys. Rev. B **96**, 075151 (2017).

[52] J.-R. Soh, H. Jacobsen, B. Ouladdiaf, A. Ivanov, A. Piovano, T. Tejsner, Z. Feng, H. Wang, H. Su, Y. Guo, Y. Shi, and A. T. Boothroyd, Phys. Rev. B **100**, 144431 (2019).

[53] G. Lee, M. A. Farhan, J. S. Kim, and J. H. Shim, Phys. Rev. B **87**, 245104 (2013).